MITSUBISHI ELECTRIC RESEARCH LABORATORIES
https://www.merl.com

Rateless Deep Graph Joint Source Channel Coding for Holographic-Type Communication

Fujihashi, Takuya; Koike-Akino, Toshiaki; Watanabe, Takashi

TR2023-139 December 04, 2023

Abstract

A key challenge in holographic-type communication is transmitting point cloud signals to users across diverse channel quality and bandwidths. Digital based point cloud coding efficiently reduces point cloud traffic. In contrast, the quantization and entropy coding in digital-based schemes causes quality degradation owing to channel quality fluctuations and diversity. This study proposes a novel scheme for point cloud delivery over wireless channels. The proposed scheme consists of a graph auto-encoder (GAE) architecture to compress the point cloud into coded symbols and restore the point cloud from the received symbols. The proposed scheme addresses the quality degradation due to channel quality fluctuations and bandwidth diversity via, the following two steps. First, the coded symbols are directly mapped onto transmission symbols, analog modulation, to ensure that the point cloud quality follows the instantaneous channel quality of each user. Second, a non-uniform dropout is introduced to realize a rateless property in the GAE architecture for gradually improving the point cloud quality according to the available bandwidth. Evaluation results demonstrate that the proposed GAE architecture can yield better point cloud quality than digital-based and analog-based schemes, even when users have varying available bandwidths.

IEEE Global Communications Conference (GLOBECOM) 2023

Mitsubishi Electric Research Laboratories, Inc.
201 Broadway, Cambridge, Massachusetts 02139

Rateless Deep Graph Joint Source Channel Coding for Holographic-Type Communication

Shoichi Ibuki*, Tsubasa Okamoto*, Takuya Fujihashi*, Toshiaki Koike-Akino†, Takashi Watanabe*
*Graduate School of Information Science and Technology, Osaka University, Osaka, Japan
†Mitsubishi Electric Research Laboratories (MERL), Cambridge, MA, USA

***Abstract*—A key challenge in holographic-type communication is transmitting point cloud signals to users across diverse channel quality and bandwidths. Digital based point cloud coding efficiently reduces point cloud traffic. In contrast, the quantization and entropy coding in digital-based schemes causes quality degradation owing to channel quality fluctuations and diversity. This study proposes a novel scheme for point cloud delivery over wireless channels. The proposed scheme consists of a graph auto-encoder (GAE) architecture to compress the point cloud into coded symbols and restore the point cloud from the received symbols. The proposed scheme addresses the quality degradation due to channel quality fluctuations and bandwidth diversity via, the following two steps. First, the coded symbols are directly mapped onto transmission symbols, analog modulation, to ensure that the point cloud quality follows the instantaneous channel quality of each user. Second, a non-uniform dropout is introduced to realize a rateless property in the GAE architecture for gradually improving the point cloud quality according to the available bandwidth. Evaluation results demonstrate that the proposed GAE architecture can yield better point cloud quality than digital-based and analog-based schemes, even when users have varying available bandwidths.**

I. Introduction

Among the latest innovations in communication technology, holographic-type communication is an attractive technique to seamlessly merge virtual and physical worlds. Holographic-type communication provides unparalleled immersion, engagement, and realism by transmitting volumetric content, such as point clouds, over wireless and mobile channels. In such channels, each user's device may experience different channel quality and have different available bandwidths owing to mobility and ambient environments. A key challenge in holographic-type communication is to deliver high quality point clouds to multiple users, even under varying channel quality and available bandwidth.

A typical solution is to employ, namely digital joint source-channel coding, where the point cloud undergoes sequential digital compression and transmission, as shown in Fig. 1 (a). For example, octree-based coding in Point Cloud Library (PCL) [1] and Kd-tree-based coding in Draco [2] can be used for digital compression. Previous studies have reported graph-based point cloud compression (PCC), which treats a point cloud as a graph signal and uses graph signal processing [3] for 3D coordinates [4] and color components [5], such as graph Fourier transform, for compression. In these studies, the 3D coordinates of a point cloud are compressed into the bitstream in a lossy manner. The transmission part

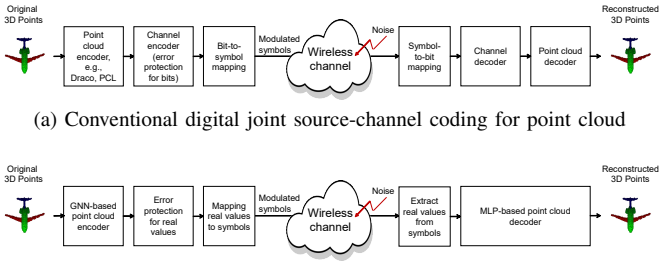

(a) Conventional digital joint source-channel coding for point cloud

(b) Proposed deep graph joint source-channel coding for point cloud

Fig. 1. Schematics of conventional and proposed schemes for point cloud delivery.

adds redundancy to the bitstream, i.e., channel coding, and then performs bit-to-symbol mapping for reliable transmission. Here, the transmitter sets source and channel coding parameters based on the measured channel quality of multiple users to fit the number of transmission symbols to the lowest available bandwidth across the users.

The combination of digital compression and transmission is optimal in point-to-point communication, as proved in Shannon's separation theorem [6]. However, it causes quality degradation of the reconstructed point cloud for multiple users owing to bandwidth heterogeneity among users and unstable wireless channel quality for each user. As mentioned above, the coding parameters were set to adjust the number of transmission symbols to the lowest available bandwidth across users to prevent playback stalls at the user. This means that, even if some users have more bandwidth, the free bandwidth is not the source of the point cloud quality improvement. The wireless channel quality instability can degrade and saturate the point cloud quality. Specifically, despite employing channel coding, the user will fail to decode the point cloud if the signal-to-noise ratio (SNR)/signal-to-interference-plus-noise ratio (SINR) of the channel falls below a certain threshold. In addition, even though some users may experience better wireless channel quality than others, the channel quality does not improve the users' point cloud quality. This is because quantization errors are not recovered on the user side.

In recent years, deep joint source-channel coding (DJSCC) schemes [7], [8] motivated by analog joint source-channel coding [9]–[13] have been proposed to overcome the problems of channel quality fluctuations. The existing DJSCC schemes use an autoencoder (AE) architecture based on deep convolutional neural networks (DCNNs) [14]–[16]. The AE

architecture encodes each image into a predefined number of coded symbols. The coded symbols are directly mapped to in-(I) and quadrature-(Q) phases as analog modulation for transmission. Next, the AE architecture reconstructs the image from the received symbols. We designed a graph AE (GAE) architecture [17] based on deep graph neural networks (GNNs) [18], [19] to perform DJSCC for holographic-type communication as shown in Fig. 1 (b). The DJSCC schemes simultaneously conduct energy compression using the AE architecture and linear mapping between the coded and transmitted symbols. Thus, the DJSCC schemes prevent decoding failure and provide good reconstruction quality according to the instantaneous channel quality.

However, in the existing AE architecture, all coded symbols have the same significance, leading to quality degradation, especially in multi-user scenarios. When the available bandwidth varies among users, the number of coded symbols in the AE architecture should be set to the widest bandwidth. In this case, users with insufficient bandwidth receive a limited number of coded symbols, resulting in a significant degradation of the reconstruction quality.

As mentioned above, the existing digital-based point cloud delivery and DJSCC schemes over wireless and mobile channels have critical issues. First, channel quality fluctuations can cause decoding failure and quality saturation Second, bandwidth diversity among multiple users can cause quality saturation and degradation. To address these problems, this paper proposes a novel DJSCC scheme for point-cloud delivery. To handle bandwidth diversity among users, the proposed scheme possesses a rateless property in the GAE architecture inspired by the weighted dropout [20]. The proposed GAE architecture employs weighted dropout during model training to adjust the importance of each coded symbol. The weighted dropout makes the significance of the coded symbols unequal. The proposed scheme can then progressively transmit the coded symbols to the users. As a result, each user gradually improves the point cloud quality according to the available bandwidth.

Evaluations using the point cloud dataset show that the linear mapping of the proposed scheme solves the quality degradation and saturation of digital-based schemes such as PCL and Draco. In addition, the rateless property in the proposed scheme gradually improves the point cloud quality according to the available bandwidth. In contrast, while the existing DJSCC scheme significantly degrades the point cloud quality for users with insufficient bandwidth to transmit all coded symbols.

The contributions of this study are four-fold:

- Our work introduces the first GAE architecture designed to handle channel quality fluctuations and bandwidth heterogeneity in holographic-type communication.
- The proposed scheme introduces the weighted dropout based on the power cumulative distribution function (CDF) during the training phase to carry out the rateless property in the proposed GAE architecture.

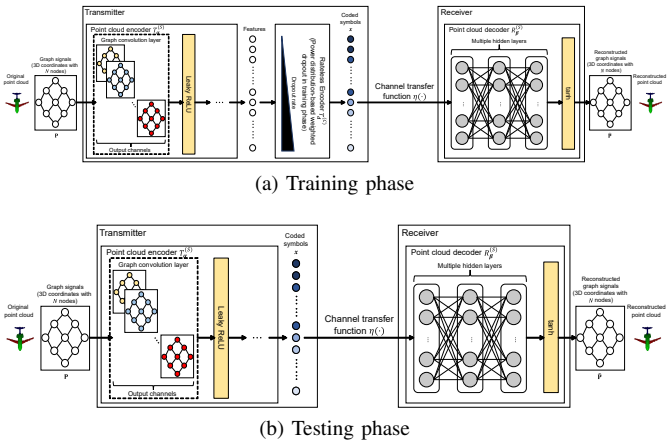

(a) Training phase

(b) Testing phase

Fig. 2. Proposed end-to-end transmitter and receiver in training and testing phases for wireless point cloud delivery.

- The proposed scheme adds a random feature [21] to each node and builds a GAE architecture with the random features further to improve the point cloud quality without additional traffic.
- A black-box optimization framework, Optuna [22], is adopted to optimize the proposed GAE architecture for point cloud quality.

II. System Model

We first introduce the considered model and the performance metric of holographic-type communication. The considered holographic-type communication system transmitted a point cloud with N 3D points at the transmitter and reconstructed the point cloud with the same number of 3D points at the receiver. The main tasks of this holographic-type communication are 1) to compress and decompress the point cloud using traditional or neural network (NN)-based encoding and decoding modules, and 2) to reconstruct the point cloud while mitigating the effects of wireless channels, such as dynamic channel quality and bandwidth diversity.

A. Transmitter

The proposed system model is shown in Figs. 2 (a) and (b). The input to the transmitter was a graph signal. Specifically, the transmitter considered a 3D point cloud as a weighted and undirected graph $\mathcal{G} = (\boldsymbol{V}, \mathcal{E}, \boldsymbol{W})$. Here, $\boldsymbol{V}$ and $\mathcal{E}$ are the sets of vertices and edges of $\mathcal{G}$, respectively. The proposed system considered 3D points as vertices in the graph, and the 3D coordinates of each 3D point $\boldsymbol{p} = [\mathrm{x}, \mathrm{y}, \mathrm{z}]^{\mathrm{T}} \in \mathbb{R}^3$ as an attribute of the vertex. In addition, a K-nearest neighbor graph was used to connect the vertices in the graph. The $\boldsymbol{W}$ is an adjacency matrix with positive edge weights. We used a binary adjacency matrix where the entry is either 1 (connection) or 0 (no connection).

The input signal is the attribute of 3D coordinates for N 3D points $\mathbf{P} = [\boldsymbol{p}_1, \boldsymbol{p}_2, \ldots, \boldsymbol{p}_N]^{\mathrm{T}} \in \mathbb{R}^{N \times 3}$. The input signal was then mapped into symbols, $\boldsymbol{x}$, to be transmitted over physical channels. The transmitter consisted of the point cloud

encoder and the rateless encoder. The point cloud encoder was implemented based on graph convolutional NNs (GCNNs), and the rateless encoder was implemented based on weighted dropout. We note that the rateless encoder was only adopted in the training phase as shown in Fig. 2 (a). By using the rateless encoder during the training phase, the coded symbols of the point cloud encoder will have a rateless property in the testing phase, as shown in Fig. 2 (b). Let the GCNN parameters of the point cloud encoder be $\boldsymbol{\alpha}$, and the distribution of the weighted dropout be d. The encoded symbol sequence, $\boldsymbol{x}$, in the training and testing phases can then be expressed as

$$\boldsymbol{x} = \begin{cases} T_{\boldsymbol{d}}^{(C)}(T_{\boldsymbol{\alpha}}^{(S)}(\mathbf{P})), & \text{training phase} \\ T_{\boldsymbol{\alpha}}^{(S)}(\mathbf{P}), & \text{testing phase} \end{cases} \tag{1}$$

where $T_{\boldsymbol{\alpha}}^{(S)}(\cdot)$ and $T_{\boldsymbol{d}}^{(C)}(\cdot)$ denote the point cloud encoder and the rateless encoder with respect to the parameter $\boldsymbol{\alpha}$ and the distribution $\boldsymbol{d}$, respectively. Here, the transmitted symbols $\boldsymbol{x}$ should be normalized to satisfy the total transmit power constraint $\mathbb{E}||\boldsymbol{x}||^2 = P$.

The normalized symbols, $\boldsymbol{x}$, were transmitted over a physical channel. The proposed system skipped the bit-to-symbol mapping and maps the symbols directly to I and Q symbols for analog modulation. The wireless channel, denoted by η, took the input $\boldsymbol{x}$ and produced the output as the received signal $\boldsymbol{y}$. If $\boldsymbol{h}$ is the channel coefficient, then the channel transfer function from the transmitter to the receiver can be modeled as

$$\boldsymbol{y} = \eta(\boldsymbol{x}) = \begin{cases} \boldsymbol{h}\boldsymbol{x} + \boldsymbol{n} & \text{received} \\ 0 & \text{missed} \end{cases} \tag{2}$$

where $\boldsymbol{n} \sim \mathcal{CN}(0, \boldsymbol{I}\sigma^2)$ is a vector of additive white Gaussian noise (AWGN) with an average noise variance of σ^2, $\boldsymbol{I}$ is an identity matrix, $\sim$ means "distributed as", and $\mathcal{CN}(a, b)$ is a complex Gaussian distribution with a mean of a and a variance of b. Here, the symbols missed because of insufficient bandwidth were treated as zeros by the receiver.

B. Receiver

The receiver was equipped with a point cloud decoder responsible for reconstructing the point cloud from the received symbols. Let the NN parameters of the point cloud decoder be $\boldsymbol{\beta}$. In this case, the decoded signal, $\hat{\mathbf{P}}$, can be obtained from the received signal, $\boldsymbol{y}$, by the following operations:

$$\hat{\mathbf{P}} = R_{\boldsymbol{\beta}}^{(S)}(\boldsymbol{y}) \tag{3}$$

where $R_{\boldsymbol{\beta}}^{(S)}(\cdot)$ is the point cloud decoder with respect to the parameters $\boldsymbol{\beta}$.

The objective of the proposed system is to reconstruct the 3D coordinates of the point cloud signal as close as possible to the original ones. The proposed system treats the point cloud decoding task as a signal reconstruction task to minimize the errors between the 3D coordinates of the point cloud $\mathbf{P}$ and the reconstructed ones $\hat{\mathbf{P}}$. The chamfer distance $\mathcal{L}_{\mathrm{CD}}(\boldsymbol{\alpha}, \boldsymbol{\beta})$ is used as the loss function of the proposed system to measure the distance between $\mathbf{P}$ and $\hat{\mathbf{P}}$ as follows:

$$\begin{aligned} &\mathcal{L}_{\mathrm{CD}}(\boldsymbol{\alpha}, \boldsymbol{\beta}) \\ &= \frac{1}{2}\Bigg\{ \frac{1}{|\mathbf{P}|} \sum_{\boldsymbol{p}\in\mathbf{P}} \min_{\hat{\boldsymbol{p}}\in\hat{\mathbf{P}}} \|\boldsymbol{p} - \hat{\boldsymbol{p}}\|_2 + \frac{1}{|\hat{\mathbf{P}}|} \sum_{\hat{\boldsymbol{p}}\in\hat{\mathbf{P}}} \min_{\boldsymbol{p}\in\mathbf{P}} \|\boldsymbol{p} - \hat{\boldsymbol{p}}\|_2 \Bigg\}, \end{aligned} \tag{4}$$

The term $\min_{\hat{\boldsymbol{p}}\in\hat{\mathbf{P}}} ||\boldsymbol{p}-\hat{\boldsymbol{p}}||_2$ enforces that each 3D coordinate $\boldsymbol{p}$ in the original point cloud $\mathbf{P}$ has a matching 3D point $\hat{\boldsymbol{p}}$ in the reconstructed point cloud $\hat{\mathbf{P}}$, and the term $\min_{\boldsymbol{p}\in\mathbf{P}} ||\boldsymbol{p} - \hat{\boldsymbol{p}}||_2$ forces the matching vice versa.

III. Proposed System

We designed a GAE architecture for holographic-type communication to solve the challenging problems due to varying channel quality and available bandwidth among multiple users. Specifically, a set of GCNNs was used for the point cloud encoder, power distribution-based weighted dropout was used for the rateless encoder, and multi-layer perceptron (MLP) was used for the point cloud decoder.

A. Point Cloud Encoder

The input of the proposed point cloud encoder, denoted as $\mathbf{P} \in \mathbb{R}^{N\times 3}$, is the 3D coordinates of the point cloud with N 3D points. The point cloud is drawn from the point cloud dataset $\mathcal{D}$. In this study, the dataset $\mathcal{D}$ consists of point clouds categorized into the same category, such as airplane, car, and bag.

Furthermore, the proposed scheme generated random features $\boldsymbol{r} \in \mathbb{R}^{N_r}$ with the number of features N_r followed by a uniform distribution. In [21], it was proven that adding random features improved the theoretical capability of GNN architectures for various tasks. Inspired by these results, random features $\mathbf{R} = [\boldsymbol{r}_1, \boldsymbol{r}_2, \ldots, \boldsymbol{r}_N]^{\mathrm{T}}$ to the input $\mathbf{P}$ as $\mathrm{CONCAT}([\mathbf{P}, \mathbf{R}]) \in \mathbb{R}^{N\times(3+N_r)}$, where $\mathrm{CONCAT}([\cdot,\cdot])$ denotes concatenation along the feature dimension.

The concatenated features were fed into the GCNN-based point cloud encoder. The point cloud encoder consists of graph convolutions and a leaky rectified linear unit (ReLU) activation function with a trainable parameter set $\boldsymbol{\alpha}$. The graph convolution layers extracted the graph signal features based on the adjacency matrix $\boldsymbol{W}$. The nonlinear activation function allows us to learn a nonlinear mapping from the source signals to the coded symbols. The point cloud encoder output the L channel features $\boldsymbol{b} \in \mathbb{R}^{N\times L}$ from $\mathbf{P}$. Here, the number of channels L depended on the graph convolutions of the proposed point cloud encoder.

B. Rateless Encoder

The rateless encoder then transformed the features $\boldsymbol{b}$ into coded symbols $\boldsymbol{x} \in \mathbb{R}^{NL}$ and fed the coded symbols to the normalization layer to normalize the power such that $\|\boldsymbol{x}\|^2 = P$.

To realize the rateless property for the coded symbols, the rateless encoder used a non-uniform dropout for the coded

symbols during the training phase. Analogously, the non-uniform dropout was performed across the width direction of the coded symbols, where independent dropouts with increasing rates are set for each coded symbol. Thus, it imposed a higher priority on the upper coded symbols during the testing phase. We note that the desired dropout rates can be achieved by adjusting the probability distribution for the non-uniform dropout. In a previous study [20], the power CDF $\Pr(D < \tau NL) = \tau^{\gamma}$, where D is the number of least principal components, τ was the compression rate, and γ was an order, was found to perform well in most cases. Accordingly, we focus on the power distribution for the dropout in the following evaluations.

The channel transfer function η took the reshaped coded symbols $\boldsymbol{x}$ as input and produced $\boldsymbol{y}$ at the receiver, which is defined in Eq. (2). In the training phase, the proposed scheme synthetically analyzed all potential distortions due to channel coefficients and additive noise. This analysis is aimed at learning optimized weights that minimize the chamfer distance over wireless channels.

C. Point Cloud Decoder

The received signal $\boldsymbol{y} \in \mathbb{R}^{NL}$ is inputted into the point cloud decoder, where it is transformed into $\hat{\boldsymbol{b}} \in \mathbb{R}^{N \times L}$. The point cloud decoder comprises a series of fully connected layers and leaky ReLU activation functions with a trainable parameter set $\boldsymbol{\beta}$. In addition, the activation function for the last layer uses the hyperbolic tangent (tanh). The point cloud decoder maps the received symbols $\hat{\boldsymbol{b}}$ into an estimate of the 3D coordinates $\hat{\mathbf{P}} \in \mathbb{R}^{N \times 3}$. The chamfer distance loss function is then computed at the receiver and propagated back to the transmitter. In this way, the trainable parameters of the point cloud encoder and decoder can be updated simultaneously.

IV. Performance Evaluation

A. Simulation Settings

Datasets: We use a benchmark dataset from ShapeNet [24] for experiments. ShapeNet contains about 17,000 3D shape point clouds from 16 shape categories. In our experiments, we select point clouds from the "Airplane" category as an example. We sample 2,115 point clouds for training and 234 for testing. The training data is used for learning the network weights, and the testing data is used for reconstruction quality comparison.

Quality Metric: We use the chamfer distance in Eq. (4) as the quality metric of the 3D coordinate attributes.

Wireless Environment: We consider AWGN channels with additive noise n_i for wireless environments. Here, the range of noise power σ^2 is from 0 dB to -30 dB. The point cloud encoder and decoder are trained in the deep graph joint source-channel coding schemes at a wireless channel SNR of 20 dB. A detailed analysis of different channel coefficients $\boldsymbol{h}$, such as Rayleigh and Rician fading coefficients, will be performed in future work.

GAE Architecture: We use PyTorch Geometric (PyG) [25] to implement our GAE architecture. Table I lists the parameter settings of the point cloud encoder, rateless encoder, and point cloud decoder in the deep graph joint source-channel coding schemes, such as the proposed scheme, the proposed scheme without random features, and GNNCast [17] found by a black-box optimization architecture Optuna [22]. The parameters minimized the chamfer distance in Eq. (4) between the original and reconstructed 3D coordinates during the training phase. Specifically, we found that GraphConv [23] was the optimal graph convolution filter among all graph convolution filters in PyG for the point cloud encoder. Additionally, the number of random features N_r was set to two. We used an adaptive momentum (ADAM) optimizer for weight learning with an initial learning rate of 0.005, batch size of 10, a momentum of 0.9, and a momentum2 of 0.999 for 200 epochs.

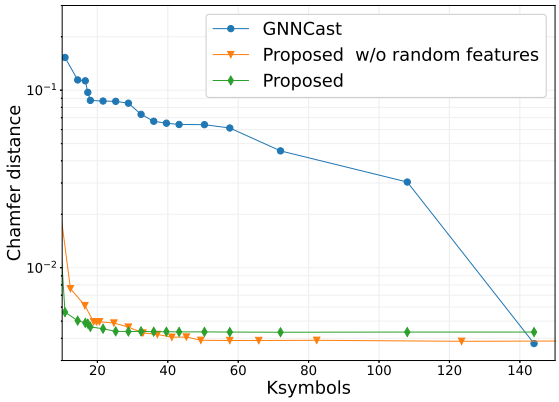

Fig. 3. Chamfer distance as a function of number of transmission symbols.

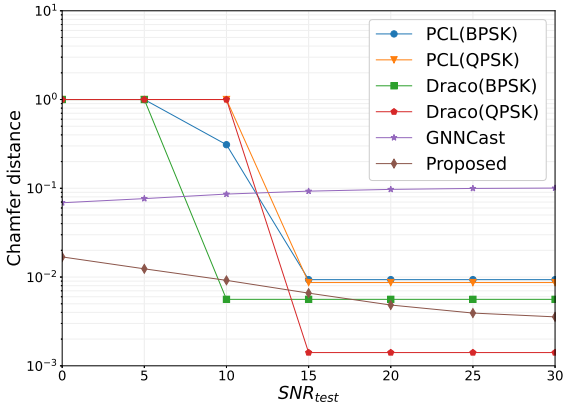

Fig. 4. Chamfer distance as a function of wireless channel SNRs.

B. Performance in Point-to-Point Environments

We first compare the baseline performance of the proposed scheme with other deep graph joint source-channel coding schemes. We prepared two baselines of the deep graph joint source-channel coding schemes: GNNCast [17] and the proposed scheme without random features. GNNCast consists of the GCNN-based point cloud encoder and MLP-based point cloud decoder. The performance improvement

TABLE I
OPTIMIZED PARAMETER SETTINGS OF THE EXISTING AND PROPOSED DEEP GRAPH JOINT SOURCE-CHANNEL CODING.

	Point cloud encoder			Rateless encoder	Point cloud decoder	
	graph convolutions	output channels in each layer	activation	order γ	output channels in each layer	activation
Proposed	GraphConv [23]	[96,32,112]	LeakyReLU	1.5	[80,128,64,64,64,32]	Leaky ReLU
Proposed w/o random features	GraphConv [23]	[80,64,32,48,128]	Leaky ReLU	1.0	[128,64,96]	Leaky ReLU
GNNCast	GraphConv [23]	[112,16,112]	Leaky ReLU	0.0	[80,96,32,48]	Leaky ReLU

from GNNCast represents the benefits of the integration with the proposed rateless encoder. The proposed scheme without random features uses the GCNN-based point cloud encoder, rateless encoder, and MLP-based point cloud decoder. The key difference between this scheme and the proposed scheme is adding random features to the input signals.

Fig. 3 shows the chamfer distance as a function of the number of transmission symbols. It is assumed that the SNR of the wireless channel is fixed at 20 dB in the testing phase. The evaluation results yield the following findings:

- GNNCast achieves the best point cloud quality with the most transmission symbols. However, the point cloud quality is significantly degraded when the number of the received symbols is limited.
- The proposed schemes with the rateless encoder can reconstruct a high-quality point cloud even though the transmitter transmits a limited number of analog modulated symbols.
- Adding random features to the input signals improves reconstruction quality for band-limited receivers.

The conducted evaluation experiments showed that the existing GNNCast is difficult to deal with the bandwidth heterogeneity, while the rateless encoder in the proposed scheme can accept the bandwidth diversity at the fixed wireless channel SNR. In practical wireless communication, the wireless channel quality often fluctuates, and the fluctuation causes quality degradation in digital-based holographic-type communication.

Here, we evaluate the effect of channel quality fluctuation on the reconstruction quality of the proposed and digital-based schemes. For performance comparison, we consider the baseline digital-based schemes based on PCL 1.12.0 [1] and Draco 1.4.3 [2]. In the digital-based schemes, each point cloud is first compressed into a bitstream using the digital encoder of PCL and Draco. The bitstream is then modulated for transmission using binary phase shift keying (BPSK) and quadrature phase shift keying (QPSK). The modulated symbols are transmitted over wireless channels and the receiver decodes the point cloud from the received modulated symbols. If the receiver fails to decode the point cloud due to bit errors, we consider the chamfer distance of the scheme to be 1.

Fig. 4 shows the chamfer distance as a function of the wireless channel SNRs. Here, the number of transmission symbols fits less than 17 K symbols in all comparison schemes for a fair comparison. The following key observations are noted:

- The proposed scheme gradually improves the chamfer distance by improving the wireless channel quality. The proposed scheme prevents decoding failure and quality saturation by skipping the digital compression and transmission.
- Draco with QPSK modulation format has better quality than the proposed scheme in high channel SNR regimes. In contrast, it fails to decode the point cloud in low SNR regimes, i.e., less than 15 dB of the channel SNR.
- PCL schemes suffer from low quality even at high channel SNRs due to low compression efficiency.

These results show that the proposed scheme may have the potential to provide a point cloud for users with low-channel SNRs.

C. Performance in Multicast Environments

The above evaluations assumed that each user requests an individual point cloud for the transmitter. In this section, we consider that multiple users request the same point cloud over wireless channels to discuss the effect of the rateless property of the proposed scheme on multicast environments. Here, there are four users and the number of receivable symbols in each user is 10, 15, 30, and 45 Ksymbols, respectively.

Figs. 5 (a) and (b) show the chamfer distance in each receiver under the wireless channel SNRs of 10 dB and 20 dB, respectively. As mentioned above, Draco needs to set the coding parameters to adjust the number of transmission symbols to the lowest available bandwidth across all users to avoid playback stalls. Even if some users can receive more digitally modulated symbols, the chamfer distance is saturated. As the proposed scheme realizes a rateless property in the analog modulated symbols. Users with narrow bandwidth, such as 10 Ksymbols, can not only reconstruct point clouds of similar quality to Draco but also users with wider bandwidth, such as 30 and 45 Ksymbols, can reconstruct better quality point clouds.

V. CONCLUSION

We have proposed a novel deep graph joint source-channel coding scheme for future holographic-type communication. Specifically, the proposed scheme integrates a GCNN-based point cloud encoder, a power CDF-based rateless encoder, an MLP-based point cloud decoder, and analog modulation to simultaneously achieve: 1) prevention of decoding failure, 2) prevention of quality saturation due to quantization, and 3) prevention of quality saturation due to bandwidth diversity among multiple users. In addition, the proposed scheme concatenates

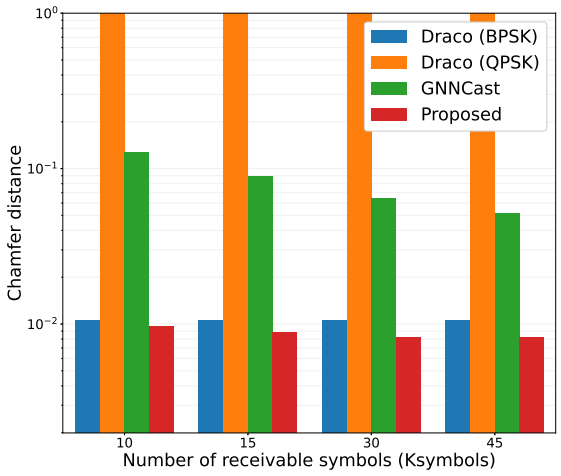

(a) Channel SNR: 10dB

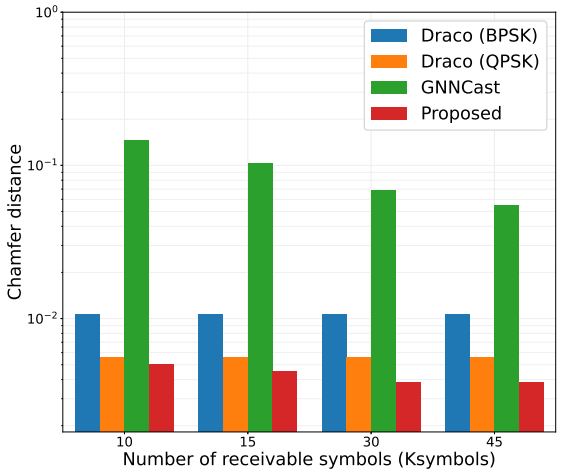

(b) Channel SNR: 20dB

Fig. 5. Chamfer distance in multicast environments with four users under the different available bandwidth.

random features along the input graph signals to enhance the rateless property realized by the proposed rateless encoder. It has been demonstrated that the proposed scheme gradually improves both the point cloud quality, with the improvement of channel quality, and the point cloud quality with wider available bandwidth in multicast environments by realizing the rateless property.

Acknowledgment

S. Ibuki's work was supported by JSPS KAKENHI Grant Numbers JP19H01101 and JP22H03582.

References

[1] J. Kammerl, N. Blodow, R. B. Rusu, S. Gedikli, M. Beetz, and E. Steinbach, "Real-time compression of point cloud streams," in *IEEE International Conference on Robotics and Automation*, 2012, pp. 778–785.

[2] "Draco 3D data compression," 2022. [Online]. Available: https://google.github.io/draco/

[3] A. Ortega, P. Frossard, J. Kovacevic, J. M. F. Moura, and P. Vandergheynst, "Graph signal processing: Overview, challenges, and applications," *Proceedings of the IEEE*, vol. 106, no. 5, pp. 808–828, 2018.

[4] P. de Oliveira Rente, C. Brites, J. Ascenso, and F. Pereira, "Graph-based static 3D point clouds geometry coding," *IEEE Transactions on Multimedia*, vol. 21, no. 2, pp. 284–299, 2019.

[5] C. Zhang, D. Florêncio, and C. Loop, "Point cloud attribute compression with graph transform," in *2014 IEEE International Conference on Image Processing (ICIP)*, 2014, pp. 2066–2070.

[6] C. E. Shannon, "Channels with side information at the transmitter," *IBM journal of Research and Development*, vol. 2, no. 4, pp. 289–293, 1958.

[7] E. Bourtsoulatze, D. B. Kurka, and D. Gunduz, "Deep joint source-channel coding for wireless image transmission," *IEEE Transactions on Cognitive Communications and Networking*, vol. 5, no. 3, pp. 567–579, 2019.

[8] H. Wu, A. Wang, J. Liang, S. Li, and P. Li, "DCSN-Cast: deep compressed sensing network for wireless video multicast," *Signal Processing: Image Communication*, vol. 76, pp. 56–67, 2019.

[9] S. Jakubczak and D. Katabi, "A cross-layer design for scalable mobile video," in *ACM Annual International Conference on Mobile Computing and Networking*, 2011, pp. 289–300.

[10] J. Shen, L. Yu, L. Li, and H. Li, "Foveation based wireless soft image delivery," *IEEE Transactions on Multimedia*, vol. 20, no. 10, pp. 2788–2800, 2018.

[11] J. Zhao, R. Xiong, and J. Xu, "Omnicast: Wireless pseudo-analog transmission for omnidirectional video," *IEEE Journal on Emerging and Selected Topics in Circuits and Systems*, vol. 9, no. 1, pp. 58–70, 2019.

[12] T. Fujihashi, T. Koike-Akino, T. Watanabe, and P. V. Orlik, "High-quality soft video delivery with gmrf-based overhead reduction," *IEEE Transactions on Multimedia*, vol. 20, no. 2, pp. 473–483, 2018.

[13] ——, "FreeCast: Graceful free-viewpoint video delivery," *IEEE Transactions on Multimedia*, vol. 21, no. 4, pp. 1000–1010, 2019.

[14] K. Zhang, W. Zuo, Y. Chen, D. Meng, and L. Zhang, "Beyond a gaussian denoiser: Residual learning of deep CNN for image denoising," *IEEE Transactions on Image Processing*, vol. 26, no. 7, pp. 3142–3155, 2017.

[15] Y. Chen and T. Pock, "Trainable nonlinear reaction diffusion: A flexible framework for fast and effective image restoration," *IEEE Transactions on Pattern Analysis and Machine Intelligence*, vol. 39, no. 6, pp. 1256–1272, 2017.

[16] Y. Tai, J. Yang, X. Liu, and C. Xu, "Memnet: A persistent memory network for image restoration," in *IEEE International Conference on Computer Vision (ICCV)*, 2018, pp. 4549–4557.

[17] T. Fujihashi, T. K. Akino, S. Chen, and T. Watanabe, "Wireless 3D point cloud delivery using deep graph neural networks," in *IEEE International Conference on Communications*, 2021, pp. 1–6.

[18] C. T. Duong, T. D. Hoang, H. H. Dang, Q. V. H. Nguyen, and K. Aberer, "On node features for graph neural networks," *arXiv e-prints*, pp. 1–6, Nov. 2019.

[19] Z. Wu, S. Pan, F. Chen, G. Long, C. Zhang, and S. Y. Philip, "A comprehensive survey on graph neural networks," *IEEE transactions on neural networks and learning systems*, vol. 32, no. 1, pp. 4–24, 2020.

[20] T. Koike-Akino and Y. Wang, "Stochastic bottleneck: Rateless auto-encoder for flexible dimensionality reduction," in *IEEE International Symposium on Information Theory (ISIT)*, 2020, pp. 2735–2740.

[21] R. Sato, M. Yamada, and H. Kashima, "Random features strengthen graph neural networks," in *Proceedings of the SIAM International Conference on Data Mining*, 2021, pp. 333–341.

[22] T. Akiba, S. Sano, T. Yanase, T. Ohta, and M. Koyama, "Optuna: A next-generation hyperparameter optimization framework," in *Proceedings of the 25th ACM SIGKDD international conference on knowledge discovery & data mining*, 2019, pp. 2623–2631.

[23] C. Morris, M. Ritzert, M. Fey, W. L. Hamilton, J. E. Lenssen, G. Rattan, and M. Grohe, "Weisfeiler and leman go neural: Higher-order graph neural networks," in *Proceedings of the AAAI conference on artificial intelligence*, vol. 33, no. 01, 2019, pp. 4602–4609.

[24] L. Yi, V. G. Kim, D. Ceylan, I.-C. Shen, M. Yan, H. Su, C. Lu, Q. Huang, A. Sheffer, and L. Guibas, "A scalable active framework for region annotation in 3d shape collections," *ACM Transactions on Graphics (ToG)*, vol. 35, no. 6, pp. 1–12, 2016.

[25] M. Fey and J. E. Lenssen, "Fast graph representation learning with PyTorch geometric," *arXiv e-prints*, Mar. 2019.